Computers in Biology and Medicine 107 (2019) 137–144

Contents lists available at ScienceDirect

Computers in Biology and Medicine

journal homepage: www.elsevier.com/locate/compbiomed

Spatially guided functional correlation tensor: A new method to associate body mass index and white matter neuroimaging

Kyoungseob Byeon[a,b,1], Bo-yong Park[a,b,1], Hyunjin Park[b,c,*]

[a] Department of Electrical and Computer Engineering, Sungkyunkwan University, Suwon, South Korea
[b] Center for Neuroscience Imaging Research, Institute for Basic Science, Suwon, South Korea
[c] School of Electronic and Electrical Engineering, Sungkyunkwan University, Suwon, South Korea

ARTICLE INFO

Keywords:
Obesity
Functional correlation tensor
Imaging biomarker
Classification
Prediction

ABSTRACT

Obesity causes critical health problems including cardiovascular disease, diabetes, and stroke. Various neuroimaging methods including diffusion tensor imaging (DTI) are used to explore white matter (WM) alterations in obesity. The functional correlation tensor (FCT) is a method to simulate DTI in WM using resting-state functional magnetic resonance imaging (rs-fMRI). In this study, we enhanced the FCT with additional anatomical information from T1-weighted data in a regression framework. The goal was to 1) develop a spatially guided enhanced FCT (s-eFCT) and to 2) use it to identify imaging biomarkers for obesity. We computed fractional anisotropy (FA) and the mean diffusivity (MD) from the s-eFCT. The regional FA and MD values that can explain body mass index (BMI) well were chosen. The identified regional FA and MD values were used to predict BMI values. The correlation between real and predicted BMIs was 0.57. There was no significant correlation between real and predicted DTI using the MD. The BMI predicted using FA was used to classify participants into three obesity subgroups. The classification accuracy was 57.20%. In summary, we found potential imaging biomarkers of obesity based on the s-eFCT.

1. Introduction

Obesity is a worldwide health problem, which is linked to many diseases including cardiovascular disease, diabetes, and stroke [1]. Body mass index (BMI) is a simple measure of obesity [2], and it is a representative measurement to assess the accumulation of body fat [3]. Previous studies found a positive correlation between BMI and morbidity suggesting that BMI might be an indicator for the physical condition of people with obesity [2,3].

Many studies found that obesity is associated with brain based on neuroimaging results of magnetic resonance imaging (MRI), positron emission tomography, and single-photon emission computed tomography (SPECT) [4–9]. MRI is an especially useful tool as it provides both structural and functional information of the brain. Diffusion tensor imaging (DTI) is one of the MRI modalities that measures the degree of water diffusion in white matter (WM). The directionality of diffusion is measured using fractional anisotropy (FA), and the magnitude of diffusion is measured using the mean diffusivity (MD). FA and the MD are the representative scalar measurements computed from DTI, and many studies adopt them to quantify the WM properties [10]. Previous neuroimaging studies found significant relationships between the WM structure alterations and obesity using DTI [11–13]. Karlsson et al. found that WM atrophy was associated with the percentage of body fat [11]. Bolzenius et al. adopted tractography analysis and found a negative correlation between BMI and the length of fibers in the temporal lobe [12]. Stanek et al. found that an increased BMI was related to decreased FA in the corpus callosum and fornix [13]. In a previous study, we predicted BMI using the structural connectivity of DTI [14]. These studies collectively suggest that obesity is related to the altered structure of WM.

Functional MRI (fMRI) that measures the blood-oxygen-level dependent (BOLD) signal from gray matter (GM) is a widely adopted neuroimaging modality in obesity-related studies [15,16]. Existing fMRI studies focused on analyzing the BOLD signal from GM [17–20]. Still, a few studies reported that significant BOLD signal existed in WM in smaller magnitude [21]. Especially, the robust signal was observed in the corpus callosum and internal capsule, parts of WM [21–24]. These studies collectively provided a basis for exploring the BOLD signal in

* Corresponding author. Center for Neuroscience Imaging Research / School of Electronic and Electrical Engineering, Sungkyunkwan University, Suwon, 16419, South Korea.
E-mail address: hyunjinp@skku.edu (H. Park).
[1] These authors contributed equally to this work.

https://doi.org/10.1016/j.compbiomed.2019.02.010
Received 7 December 2018; Received in revised form 28 January 2019; Accepted 14 February 2019

the WM. A method to explore BOLD signals from WM using fMRI was proposed by Ding et al. [25]. They developed a method known as the functional correlation tensor (FCT) to mimic DTI [25,26]. The FCT was constructed by calculating the correlations of time courses between a given voxel and its adjacent voxels, and then the correlation values were further modified with a dyadic tensor. Ding et al. reconstructed the neuronal fibers in the corpus callosum and optic radiation using FCT suggesting the possibility of developing pseudo-DTI from fMRI [25]. This might allow us to extract DTI like information from fMRI data and thus might save the scanning time as there is less need to perform real DTI data acquisition. The decrease in the scanning time can be an important factor for children and elderly subjects who might have difficulties with staying in the scanner for an extended period of time, which is required for multimodal acquisition studies.

In this study, we aimed to achieve two goals. First, we aimed to enhance the FCT by incorporating spatial information of T1-weighted structural data. We hypothesized that the spatial information might provide complementary information for constructing the FCT. Second, we aimed to find biomarkers of obesity using a spatially guided enhanced FCT (s-eFCT). We predicted BMI using the s-eFCT. We hypothesized that the s-eFCT might be used as imaging biomarkers to distinguish among subclasses of obesity.

2. Materials & methods

2.1. Subjects and imaging data

The institutional review broad (IRB) of Sungkyunkwan University approved our study. Consent was waived for this retrospective study. Our study was performed in full accordance with local IRB guidelines. We obtained DTI, resting-state functional magnetic resonance imaging (rs-fMRI), and T1-weighted data from enhanced Nathan Kline Institute-Rockland sample (NKI-RS) database Release 1–8 [27]. All NKI-RS participants were scanned on a Siemens Magnetom Trio Tim scanner with the following imaging parameters. For fMRI, the parameters were the repetition time (TR) = 645 ms, echo time (TE) = 30 ms, field of view (FOV) = 222 mm, flip angle = 60°, 900 vol, and isotropic slice size = $3 \times 3 \times 3\,mm^3$. For DTI, the parameters were the TR = 2400 ms, TE = 85 ms, FOV = 212 mm, flip angle = 90°, isotropic slice size = $2 \times 2 \times 2\,mm^3$, b value = $1500\,s/mm^2$, and 137 directions. Of the total 771 subjects, subjects without BMI information, T1-weighted data, rs-fMRI, or DTI data were excluded. The subjects with severe distortions in DTI reconstructions were also excluded. We randomly selected 88 subjects for each group from the remaining 305 subjects: healthy weight (HW), overweight (OW), and obesity (OB). The OB group had only 88 subjects and thus we randomly chose 88 subjects in the other two groups to balance the number of samples in each group. The three groups were classified using the WHO BMI criteria [28]. Non-imaging data such as age, sex and BMI were obtained from the database.

2.2. Data preprocessing

The T1-weighted and rs-fMRI data were preprocessed using FSL and AFNI software [29,30]. For the T1-weighted data, we removed the skull and registered them onto Montreal Neurological Institute (MNI) standard space. The rs-fMRI data were processed as follows. The first 10 s (16 vol) were removed to adjust for the hemodynamic response delay. Head motion and slice timing effects were corrected. Intensity normalization was applied as a mean value of 10,000 across the data. The fMRI data were registered onto the high-resolution T1-weighted data and then subsequently registered onto the $3\,mm^3$ MNI standard space. A low pass filter with a cutoff of 0.1 Hz was applied to remove noise and keep WM signals. Spatial smoothing was not performed because it could introduce artificial spatial correlation, which might negatively affect the computation of the FCT. Preprocessing of the DTI data was performed using FSL and diffusion toolkit (DTK) software [31]. Non-brain tissues of raw DTI data were removed. The raw DTI data were registered onto the image with a b value of s/mm^2 and then subsequently registered onto the $3\,mm^3$ MNI standard space. The reconstruction of the DTI data was performed with the standard diffusion tensor model using the DTK software [31].

2.3. Functional correlation tensor

To compute the FCT, only the BOLD signals located in WM from fMRI were used. Inspired by Ding et al. the tensor T_i of a voxel V_i was calculated as follows [26]:

$$T_i = \sum_{j=1}^{26} w_{ij} D_{ij} \tag{1}$$

where w_{ij} was the soft threshold-weighted Pearson correlation coefficient between the time series of V_i and V_j as equation (2) [26,32].

$$w_{ij} = \left(\frac{(r_{ij}+1)}{2}\right)^{\beta} \tag{2}$$

where r_{ij} was the correlation value of the time series between voxels V_i and V_j. We adopted the soft-thresholding method for the correlation value using the scale-free index β, which was set to 12. D_{ij} was the dyadic tensor constructed with the unit vector $n_{ij} = [n_{ij,x}, n_{ij,y}, n_{ij,z}]^T$ between V_i and V_j [26,33,34]:

$$D_{ij} = n_{ij} n_{ij}^T = \begin{bmatrix} n_{ij,x}n_{ij,x} & n_{ij,x}n_{ij,y} & n_{ij,x}n_{ij,z} \\ n_{ij,x}n_{ij,y} & n_{ij,y}n_{ij,y} & n_{ij,y}n_{ij,z} \\ n_{ij,x}n_{ij,z} & n_{ij,y}n_{ij,z} & n_{ij,z}n_{ij,z} \end{bmatrix} \tag{3}$$

For a voxel V_i in the brain WM, a total of 26 voxels adjacent in 3D are defined as V_j. The procedure above is referred to as the construction of the FCT.

2.4. Enhancement of the FCT

The FCT was further enhanced using a multivariable linear regression framework to resemble the real diffusion tensor. The directional values of FCT and T1-weighted intensity values were set as independent variables and one direction of the diffusion tensor from real DTI as dependent variable:

$$\widehat{DT_i} = \sum_{j=1}^{6} \alpha_j FCT_j + \sum_{k=1}^{6} \beta_k A_k + \varepsilon \tag{4}$$

where FCT_j and A_k were the FCT in each direction and the anatomical T1-weighted value in the neighborhood, respectively. α_j and β_k were the corresponding regression coefficients, and ε was the regression error. $\widehat{DT_i}$ was the simulated diffusion tensor in each direction using the s-eFCT. The neighbors of the T1 data were four in-plane neighbors and two out-of-plane neighbors. The process was repeated for all six components of the diffusion tensor. We used the s-eFCT to calculate the FA and the MD of the simulated diffusion tensor, which were compared with those from real DTI. FA was derived from the three eigenvalues (λ_1, λ_2, λ_3) of the s-eFCT. MD was calculated as the sample mean of the three eigenvalues as follows,

$$MD = \frac{\lambda_1 + \lambda_2 + \lambda_3}{3} \tag{5}$$

FA was calculated as,

$$FA = \sqrt{\frac{3}{2}} \sqrt{\frac{(\lambda_1 - \hat{\lambda})^2 + (\lambda_2 - \hat{\lambda})^2 + (\lambda_3 - \hat{\lambda})^2}{\lambda_1^2 + \lambda_2^2 + \lambda_3^2}} \tag{6}$$

where $\hat{\lambda}$ was MD. The region-wise mean values of FA and MD were computed for 50 WM regions based on the ICBM DTI-81 atlas available on the standard space [35].

2.5. Feature selection for BMI prediction

We used the s-eFCT to calculate the mean values of FA and MD for the 50 WM regions. The FA or MD values that could explain BMI well were selected using the least absolute shrinkage and selection operator (LASSO) framework [36]. The LASSO is a regularized regression analysis, which can select a sparse set of variables that can explain the dependent variable well. The LASSO was applied to 50 FA values and 50 MD values separately. The selected variables were encouraged to be orthogonal.

2.6. BMI prediction

A multivariable linear regression model was created using the mean FA or MD values of the identified regions as independent variables and the actual BMI values as dependent variables. From two-sample t-tests for every combination of groups, age showed group differences (see the details in the Result section). Thus, the age was added as a covariate for the linear regression model.

$$BMI = \sum_{i=1}^{N} \beta_i FA_i + \gamma \cdot age + \varepsilon \quad (7)$$

where FA_i were the regional FA values, and γ was regression coefficient, N was the number of selected imaging features, and ε was the error. The prediction was performed in a 10-fold cross-validation fashion. For each left out test fold, remaining nine training folds were used to identify features via the LASSO. We classified the predicted BMI of the left out test fold into three subgroups (i.e., HW, OW, and OB) according to the obesity criteria [2] using the identified features from the LASSO. We compared the predicted subgroup assignment with the ground truth label using a 3×3 confusion matrix. The process was repeated 10 times each time leaving a different fold out.

2.7. Statistics

A 10-fold cross-validation was adopted separating the training and the test data. The regression coefficients were computed from nine training folds, and we reserved one fold as testing in later stages. The process was repeated 10 times each time leaving a different fold out. To enhance the original FCT, a multivariable linear regression model was constructed. In the regression model, we used 12 independent variables including six-directional values of the FCT and six (i.e., the six immediate neighbors of the voxel) T1-weighted intensity values. As a dependent variable, one direction of the diffusion tensor from real DTI was used. To select the features to explain BMI, the LASSO framework was adopted. Additional multivariable linear regression models were created using the mean FA or MD values of the identified regions as independent variables and the actual BMI values as dependent variables. From two-sample t-tests for every combination of groups, age showed group differences (see details in the Results section). Thus, the age was added as a covariate for the linear regression model. The prediction was performed in a 10-fold cross-validation fashion. For each left out test fold, remaining nine training folds were used to identify features via the LASSO. We applied the LASSO 10 times for 10 different training dataset to select significant regional FA/MD features. Prediction results were quantified using the Pearson correlation and intraclass correlation (ICC) between the actual and predicted BMIs. The error of the prediction was assessed using the root mean squared error (RMSE). The predicted BMI was classified into three subgroups (i.e., HW, OW, and OB) and compared with the ground truth label. The result of the three-subgroup classification using the predicted BMI was measured using precision, recall, F1-score, and accuracy. The reported classification performances were derived from overall confusion matrix calculated by summation of 10 left out test folds. The reported classification performances were averaged values of 10 left out test folds. The s-eFCT construction, feature selection, and prediction were conducted using Python (version 2.7. Python Software Foundation. Python Language reference). Pearson correlation and RMSE were calculated using MATLAB (version 2016b, MathWorks Inc. Natick, MA, USA). The ICC was computed using SPSS (version 20.0., IBM SPSS Statistics for Windows, Armonk, NY: IBM Corp.).

Table 1
Subject information for the three-subgroups depending on the BMI.

Group	BMI Range	number of subjects (M: F)	Mean (SD) Age	Mean (SD) BMI
HW	18.50 – 24.99	88 (28:60)	34.96 (14.03)	22.50 (1.64)
OW	25.00 – 29.99	88 (34:54)	38.10 (13.82)	27.39 (1.38)
OB	≥ 30.00	88 (29:59)	41.52 (12.22)	35.10 (4.58)
P-value[a]	-	0.3437[b]	0.001	< 0.001

Notes.
HW, healthy weight; OW, overweight; OB, obesity; M, male; F, female; BMI, body mass index; SD, standard deviation.
[a] P-values were reported for the lowest value.
[b] Chi-squared test for the sex ratio.

3. Results

3.1. Study participants

We considered 264 subjects in this study. The subjects were classified into three subgroups of HW, OW and OB groups. Detailed demographic information is described in Table 1 for all three subgroups.

3.2. Quality of the s-eFCT

We constructed the s-eFCT using the fMRI with T1-weighted data and calculated the FA and MD values for the WM regions. The tensors were compared with those of the real diffusion tensor and the s-eFCT using Pearson's correlation in the 10-fold cross-validation. The mean correlation of the tensors over six channels of all regions of interest (ROIs) between the s-eFCT and the diffusion tensor was 0.39 (Table S1). The mean correlation between the FA values derived from the diffusion tensor and the s-eFCT was 0.36, and that of the MD values was 0.47. The results for FA and MD of each ROI were reported in Table S2.

3.3. Selected imaging features from the LASSO

The selected imaging features to explain BMI were reported in Fig. 1. As we adopted the 10-fold cross-validation, the selected features were slightly different among different folds. We kept the ones that were selected all 10 times. Fig. 1 showed the features that were commonly identified from all 10 folds. The LASSO method identified 26 ROIs using the FA values. The regions included regions of major fiber bundles, such as the corpus callosum (CC), fornix (FX), medial lemniscus (ML), internal capsule (IC), corona radiata (CR), fronto-occipital fasciculus (FO), cerebellar peduncle (CP), and cingulum including cingulate gyrus (CGC) and hippocampus (CGH). The identified regions, CC, FX, ML, IC, CR, FO, CGC, and CGH were the previously reported regions associated with BMI [37–42]. Thus, the identified regions were mainly consistent with the known literature of obesity. The detailed regions were reported in Fig. 1. The LASSO method identified 13 ROIs using the MD values consistently. They were the genu, body, and splenium of CC, FX, left ML, right cerebral peduncle, right anterior limb and left retro part of IC, both side of posterior thalamic radiation, left CGC, left CGH, and right uncinate fasciculus.

3.4. Comparison between the real and predicted BMI

The identified regions and the associated FA values were used as

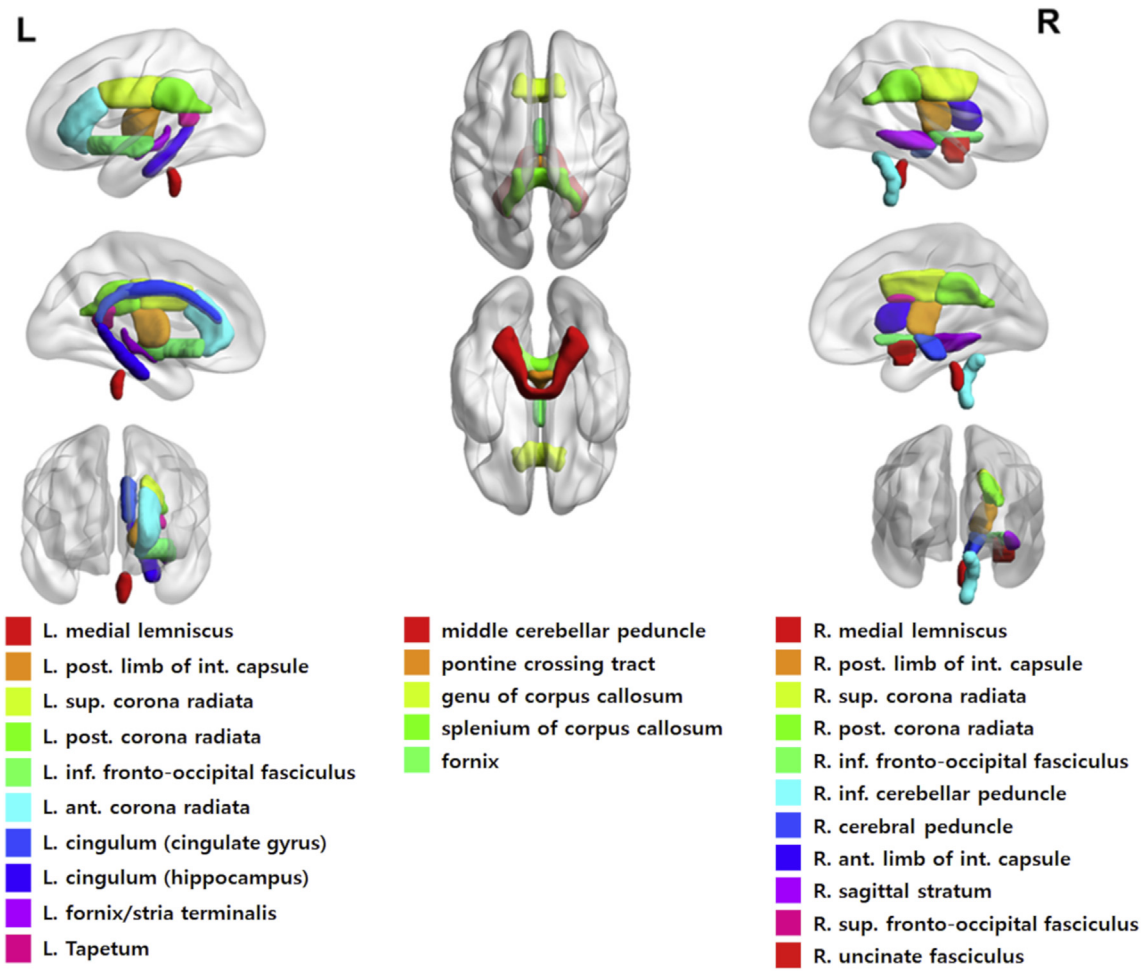

Fig. 1. Identified 26 regions via the LASSO feature selection using FA to explain BMI. The left and right subfigures show regions of each hemisphere. The middle column shows regions located in.

independent variables in a multivariate linear regression framework to predict the BMI values in a 10-fold cross-validation fashion. The predicted BMI and actual BMI values showed a meaningful correlation (mean r = 0.57) over 10 left out test folds. The mean (standard deviation [SD]) RMSE between the predicted and actual BMIs was 4.96 (0.65). The mean (SD) ICC was 0.67 (0.19). There was no association between the BMI predicted using the MD and the actual BMI values. The detailed result of comparison between the real BMI and predicted BMIs was described in Table 2.

3.5. Subgroup classification

We used FA of the identified regions from the s-eFCT to perform classification of subjects into three subgroups. The accuracy of the classification was evaluated by the ratio of the true label to the whole label. The mean of the classification accuracy using the FA values of the identified regions among 10 left out test folds was 57.31%. The baseline accuracy (i.e., blinding assigning all cases to the dominant label) of the classification was 33.33% owing to the balanced number of samples in each subgroup. The detailed results of the classification were described in Table 3.

3.6. Comparison with DTI

To compare the prediction results from s-eFCT, we additionally performed BMI prediction using real DTI. The LASSO method identified nine regions of the genu of CC, right ML, IC (right anterior limb, left posterior limb, left retrolenticular part), right posterior thalamic radiation, right CGC, right uncinate fasciculus, and left tapetum using FA. When MD was used, three regions of the body of CC, right posterior thalamic radiation, and right uncinate fasciculus were identified. There were significant correlations between the predicted and actual BMI using FA on six out of ten folds (Table 4). The mean accuracy of the classification was 46.59% (Table 5). When MD was used, most folds showed low correlation and classification accuracy (Tables 4 and 5).

4. Discussion

In the current study, we aimed to develop a new variant of the FCT, the s-eFCT, which contains both functional and structural brain information using fMRI and T1-weighted data. The functional information was measured by correlating temporal fluctuations in fMRI between all pair of voxels in the WM. The structural information was voxel-wise T1-weighted data. We used our s-eFCT to predict the BMIs of people with a wide range of BMI values, and it led to fair prediction results (mean r = 0.57). The predicted BMI score was used to perform a three-label classification of the BMI subgroups.

Several recent studies suggested the use of the FCT as an imaging biomarker to distinguish patients with mild cognitive impairment (MCI) from normal controls [43,44]. Zhang et al. performed classification between early-stage MCI and normal controls using the FA map calculated from FCT as the discriminating features [43]. Their work focused on Alzheimer's disease, while ours focused on obesity. We enhanced the FCT with anatomical T1 information and fMRI, while their

Table 2
Comparison between the real and predicted BMI using the s-eFCT. The Pearson's and intraclass correlation values were computed between the real and predicted BMI. The regression line is between the real and predicted BMI.

feature	Fold	Pearson's correlation		Intraclass correlation			Regression Line		RMSE
		r	p	r	95% CI	p	β	ε	
FA	1	0.66	< 0.001	0.69	0.31–0.86	0.020	1.34	-9.18	5.53
	2	0.57	0.002	0.71	0.36–0.87	0.010	0.75	7.77	4.94
	3	0.63	< 0.001	0.75	0.44–0.88	< 0.001	0.89	2.63	4.56
	4	0.11	0.601	0.16	-0.85–0.62	0.334	0.21	22.27	5.86
	5	0.66	< 0.001	0.79	0.54–0.91	< 0.001	0.77	5.84	4.19
	6	0.40	0.038	0.56	0.36–0.80	0.020	0.32	19.40	6.19
	7	0.77	< 0.001	0.85	0.68–0.93	< 0.001	1.01	−1.71	4.19
	8	0.67	< 0.001	0.76	0.46–0.89	< 0.001	1.04	-1.48	4.58
	9	0.73	< 0.001	0.79	0.52–0.91	< 0.001	1.16	-5.00	4.73
	10	0.49	0.016	0.59	0.06–0.82	0.018	0.85	4.50	4.84
	Mean	0.57	-	0.67	-	-	0.83	-	4.96
	SD	0.18	-	0.18	-	-	0.32	-	0.62
MD	1	0.57	0.002	0.55	0.01–0.80	0.023	1.49	−11.8	6.24
	2	0.4	0.040	0.48	-0.13–0.77	0.049	0.79	5.86	5.31
	3	0.43	0.024	0.50	-0.11–0.77	0.043	0.93	0.32	5.51
	4	−0.01	0.942	−0.22	-1.24–0.53	0.522	-0.03	28.79	6.02
	5	0.59	0.001	0.74	0.42–0.88	0.001	0.73	6.19	4.71
	6	0.3	0.128	0.44	-0.22–0.75	0.072	0.42	16.3	5.09
	7	0.58	0.002	0.54	-0.02–0.79	0.027	1.62	-17.42	5.31
	8	0.48	0.011	0.49	-0.12–0.77	0.045	1.24	-5.76	5.46
	9	0.47	0.020	0.44	-0.31–0.76	0.089	1.45	-11.49	6.15
	10	0.05	0.831	0.07	-1.16–0.60	0.437	0.11	25.01	5.96
	Mean	0.39	-	0.40	-	-	0.88	-	5.58
	SD	0.20	-	0.26	-	-	0.55	-	0.48

CI, confidence interval; β, regression coefficient; ε, regression intercept; RMSE, root mean square error; SD, standard deviation.

Table 3
Three subgroup classification results using the BMI predicted by the FA or MD of the s-eFCT. Table entries are the sum of performance measures over 10 left out folds.

Truth	Prediction							
	FA				MD			
	HW	OW	OB	Mean	HW	OW	OB	Mean
HW	37	38	13	-	11	67	10	-
OW	8	60	20	-	10	63	15	-
OB	7	27	54	-	5	48	35	-
Precision (%)	71.15	48.00	62.07	60.41	42.31	35.39	58.33	45.34
Sensitivity (%)	42.05	68.18	61.36	57.20	12.50	71.59	39.77	41.29
Specificity (%)	52.86	56.34	61.71	56.97	19.30	47.37	47.30	37.99
Accuracy (%)	57.20				41.29			

HW, healthy weight; OW, overweight; OB, obesity.

enhancement approach only used information from fMRI. They used regression forest, while we used linear regression to enhance the FCT. Chen et al. used the FCT method with a dynamic sliding window approach and performed the classification between MCI and normal controls [44]. Their approach did not include the enhancement of the FCT. Using the sliding window, they computed dynamic functional connectivity and that resulted in having more features (i.e., many connectivity values instead of one static connectivity value). The approach might require more samples as the complexity of the model increased significantly. Zhou et al. suggested the FCT could be used for image registration [34]. They demonstrated that the performance of the brain image registration could be improved using the FCT as a new feature to drive the image registration procedure. Their approach did not enhance the FCT and has a very different application domain.

The FCT was constructed by considering the functional association of the time series between different voxels, and it did not lead to good similarity with the real diffusion tensor (Table S1). Thus, we further explored whether a simple linear regression framework can enhance the FCT to resemble the real diffusion tensor better with more factors. The FCT contained six channels of information, which might jointly contribute the real diffusion tensor. For example, the dxx (major horizontal component) of real DTI might contain contributions from different combinations of six channels of the FCT. We considered all six channels of the FCT to model each directional component of the real diffusion tensor to construct an enhanced FCT (eFCT) model. However, the eFCT using only six channels of information of the FCT still did not reflect patterns of the real diffusion tensor well. We hypothesized that this might be due to the absence of the anatomical information, which is difficult to obtain from BOLD signals. Thus, we included the T1-weighted intensity values of the six neighbors of the given voxel to improve the FCT model. This could be thought of as extending the original FCT model of Ding et al. by adding anatomical information. We compared three versions of the FCT (i.e., original FCT, eFCT, and s-eFCT). We found that the similarity between the s-eFCT with anatomical information and the real diffusion tensor revealed the highest correlation value in WM (mean r = 0.38) followed by the eFCT and the original FCT (Table S1).

We identified 26 regions related to the BMI from 50 WM regions. Existing DTI studies of obesity also identified many of the same regions we identified. Some studies found a relationship between the body fat indices and changes in FA in WM using DTI [11,37,39–41]. Raji et al. reported that there was atrophy in the CR in the OW group compared to the HW group [37]. They also found that the OB group showed atrophy in the subcortical WM regions of the CGC and CGH [37]. Papageorgiou et al. associated the brain fiber and obesity using tract-based spatial statistics [39]. They found that FA of the OW group was decreased in the CGC and CGH. They also found that FA of the OB group was decreased in the inferior FO, CC, unicate fasciculus, and IC [39]. Xu et al. reported a relationship between the BMI and FA, MD, axial eigenvalues, and radial eigenvalues in each of the CC, FX, and CR [40]. The report of Verstynen et al. showed that FA is associated with the BMI over most of the WM regions [41]. Especially the CP and ML showed a high correlation with the BMI [41].

We performed the subgroup classification using the selected brain regions. The classification precisions in the HW (71.15%) and OB (62.07%) groups were higher than the OW (48.00%) group. The OW

Table 4
Comparison between the real and predicted BMI using the DTI. The Pearson's and intraclass correlation values were computed between the real and predicted BMI. The regression line is between the real and predicted BMI.

feature	Fold	Pearson's correlation		Intraclass correlation			Regression Line		RMSE
		r	p	r	95% CI	p	β	ε	
FA	1	0.83	< 0.001	0.80	0.56–0.91	< 0.001	1.67	−17.97	4.72
	2	0.37	0.056	0.46	−0.19–0.75	0.063	0.75	6.65	5.41
	3	0.45	0.019	0.57	0.06–0.81	0.017	0.73	6.54	5.45
	4	0.05	0.790	0.09	−1.00–0.58	0.409	0.1	25.22	6.03
	5	0.59	0.001	0.70	0.45–0.86	0.001	0.88	2.75	4.37
	6	0.34	0.085	0.47	−0.17–0.76	0.056	0.53	13.27	4.84
	7	0.5	0.007	0.54	−0.01–0.79	0.027	1.16	−3.81	5.49
	8	0.45	0.019	0.51	−0.07–0.78	0.036	0.96	2.11	5.57
	9	0.65	0.001	0.66	0.21–0.85	0.006	1.41	−11.22	5.36
	10	0.36	0.081	0.39	−0.41–0.74	0.123	0.96	0.97	5.14
	Mean	0.46	-	0.52	-	-	0.92	-	5.24
	SD	0.20	-	0.18	-	-	0.42	-	0.46
MD	1	0.48	0.012	0.43	−0.26–0.74	0.081	1.51	−14.04	6.41
	2	−0.01	0.977	−0.01	−1.21–0.54	0.506	−0.02	28.98	5.94
	3	0.29	0.146	0.27	−0.61–0.67	0.218	1	−0.77	5.62
	4	0.07	0.740	0.06	−1.05–0.57	0.434	0.25	20.92	5.5
	5	0.57	0.002	0.59	0.09–0.81	0.014	1.32	−10.13	4.49
	6	0.33	0.091	0.45	−0.20–0.75	0.066	0.55	12.63	4.8
	7	0.26	0.188	0.25	−0.65–0.66	0.238	0.89	3.68	6.11
	8	0.58	0.002	0.36	−0.40–0.71	0.130	2.9	−52.33	5.57
	9	0.34	0.099	0.34	−0.53–0.72	0.163	1.05	−1.4	6.39
	10	−0.1	0.628	−0.10	−0.16–0.52	0.591	−0.42	39.98	5.82
	Mean	0.28	-	0.26	-	-	0.90	-	5.67
	SD	0.22	-	0.21	-	-	0.88	-	0.60

CI, confidence interval; β, regression coefficient; ε, regression intercept; RMSE, root mean square error; SD, standard deviation.

Table 5
Three subgroup classification results using the BMI predicted by the FA or MD of the DTI. Table entries are the sum of performance measures over 10 left out folds.

Truth	Prediction							
	FA				MD			
	HW	OW	OB	Mean	HW	OW	OB	Mean
HW	18	58	12	-	3	79	6	-
OW	10	61	17	-	2	79	7	-
OB	6	38	44	-	2	67	19	-
Precision (%)	52.94	38.85	60.27	50.69	42.86	35.11	59.38	45.78
Sensitivity (%)	20.45	69.32	50.00	46.59	3.41	89.77	21.59	38.26
Specificity (%)	86.78	39.24	73.15	66.39	96.08	13.10	86.32	65.16
Accuracy (%)	46.59				38.26			

Notes.
HW, healthy weight; OW, overweight; OB, obesity.

group lies between HW and OB groups in BMI values and the errors could occur if the predicted BMI is lower than the threshold of 25 or higher than the threshold of 30. For HW and OB groups, errors could only occur in one direction toward the OW group. This led to having lower precision for the OW group. On the other hand, the recall of OW (68.18%) and OB (61.36%) groups were higher than HW (42.05%) group as many subjects in the HW group were erroneously classified as OW or OB. This might indicate it is difficult to distinguish between the HW and OW groups. The F1-score was the highest in the OB group possibly suggesting that our model explained the people with obesity well compared to the other two groups.

We predicted the BMI using real DTI to compare with the s-eFCT approach. The selected imaging features using FA and MD of DTI included CC, ML, IC, and CGC. These regions were previously reported in our s-eFCT experiment. The mean accuracy of the classification using the predicted BMI using FA of DTI was 46.59%, which was lower than that using the s-eFCT (57.20%). A majority of folds in the MD prediction showed no significant correlation, and it did not classify the BMI subgroups well. One possible reason could be that our s-eFCT combined functional information of fMRI with the anatomical T1-weighted information thus could be a more useful biomarker to explain BMI than approaches using only DTI.

The MD predicted using the s-eFCT was more correlated with the actual MD than FA predicted with actual FA (Table S2). Nevertheless, the BMI predicted using the MD hardly classified the three subgroups. Pearson's correlation between the predicted MD and the actual MD showed significant similarity in seven out of ten folds (Table 2), but the mean accuracy of the classification among ten folds was only 41.39%, close to the baseline accuracy. The prediction of the MD using real DTI also showed a low performance, so we found that the mean eigenvalues of the tensor had little or no involvement in the change of the BMI. The results indicate that the directionality of diffusion modeled with the FCT is different from the real diffusion tensor, and it explained the BMI of HW, OW, and OB better. The reason why the directionality of diffusion is better at predicting the BMI than the magnitude of diffusion needs further validations.

In this study, we matched the number of subjects in each class. Machine learning approaches work well when we have a balanced number of subjects in each class [45]. The OB group had the least number of subjects and thus randomly subsampled the other two groups (HW and OW) to have the same number of subjects. We could have lost a large amount of information due to this subsampling and thus we applied random subsampling 10 times more and reported the stability of our results. For each new set of patients, we constructed the s-eFCT, which was further used to compute FA values. The regions identified in the new 10 sets were largely consistent with those reported in the main text (Table S3). Among the 26 regions identified in the main text, we observed that 15 regions were also found at least eight times in the new 10 sets. In addition, we quantified the classification performance using the FA values. The classification performances from the new 10 sets were similar to those reported in the main text (Table S4). The mean correlation between the predicted BMI and real BMI was 0.56 (SD = 0.02) and this was similar to the results of the main text (r = 0.57). The mean classification accuracy was 55.63% (SD = 2.81) and it was also similar to the result of the main text (57.20%).

We explored using other DTI related measures from the s-eFCT to improve the classification performance. Besides the FA and MD tested, we computed 50 regional axial diffusivity (AD), radial diffusivity (RD), relative anisotropy (RA), and volume ratio (VR) from our s-eFCT. Those measures were subjected to the same LASSO approach to retain significant features related to BMI. Using these measures for classification did not result in better classification performances than using FA alone (Table S5). Our classification model is based on the linear regression model and thus there is a room for improvements. In particular, deep learning methods could be used for improving the accuracy of the classification and is left for future research.

Our study has several limitations. There is a lack of meaningful studies reporting on the BOLD signal activity in the WM areas other than the corpus callosum and internal capsule. Our study found many other WM regions besides the two. Thus, the regions we found in this study related to the BMI need to be further validated in an independent setting. BMI is an indirect indicator for the measurement of obesity. Some changes in the brain composition that occur with obesity might not be measured by the BMI owing to low sensitivity and specificity of BMI as a measure of obesity [46]. However, future studies need to take a more stable and direct clinical score of obesity. We did not model the underweight (UW) group since the NKI-RS database did not have sufficient samples in the UW group. Our study adopted machine learning approaches and it is important to have sufficient samples in each group. Further studies are needed with more samples in the UW group. We adopted a simple linear regression model so that the obtained model is easily interpretable and generalizable to other cases compared to other high degree of freedom non-linear models. There is a room for improvements in particular by using deep learning methods. Deep learning is a promising technique, which could be used for improving the accuracy of the classification. This is beyond scope of the current study and is left for future research.

5. Conclusions

In this study, we combined the FCT and T1-weighted anatomical information to construct our s-eFCT in a regression framework to model the diffusion tensor. The s-eFCT model was used to compute the FA and MD values of the WM regions. We identified FA and MD of the WM regions related to BMI, which were used as input of a BMI score prediction model. The correlation between the real and predicted BMIs was 0.57. We divided the predicted BMI to distinguish between three subgroups of obesity. The classification accuracy was 57.20%. In summary, we found imaging biomarkers of obesity based on the s-eFCT.

Acknowledgments

This study was supported by the Institute for Basic Science (grant number IBS-R015-D1), the National Research Foundation of Korea (grant numbers NRF-2016R1A2B4008545 and NRF-2016H1A2A1907833), and the Ministry of Science and ICT of Korea under the ITRC program (IITP-2018-2018-0-01798). Imaging data were obtained from the NKI-RS database.

Appendix A. Supplementary data

Supplementary data to this article can be found online at https://doi.org/10.1016/j.compbiomed.2019.02.010.

References

[1] C.J. Lavie, R.V. Milani, H.O. Ventura, Obesity and cardiovascular disease. Risk factor, paradox, and impact of weight loss, J. Am. Coll. Cardiol. 53 (2009) 1925–1932, https://doi.org/10.1016/j.jacc.2008.12.068.

[2] F.Q. Nuttall, Body mass index: obesity, BMI, and health: a critical review, Nutr. Today 50 (2015) 117–128, https://doi.org/10.1097/NT.0000000000000092.

[3] K.E. Bradbury, W. Guo, B.J. Cairns, M.E.G. Armstrong, T.J. Key, Association between physical activity and body fat percentage, with adjustment for BMI: a large cross-sectional analysis of UK Biobank, Br. Med. J. Open 7 (2017), https://doi.org/10.1136/bmjopen-2016-011843 e011843.

[4] K.C. Willeumier, D.V. Taylor, D.G. Amen, Elevated BMI is associated with decreased blood flow in the prefrontal cortex using SPECT imaging in healthy adults, Obesity 19 (2011) 1095–1097, https://doi.org/10.1038/oby.2011.16.

[5] G.J. Wang, N.D. Volkow, J. Logan, N.R. Pappas, C.T. Wong, W. Zhu, N. Netusil, J.S. Fowler, Brain dopamine and obesity, Lancet 357 (2001) 354–357 doi:16/S0140-6736(00)03643-6.

[6] K.S. Burger, L.A. Berner, A functional neuroimaging review of obesity, appetitive hormones and ingestive behavior, Physiol. Behav. 136 (2014) 121–127, https://doi.org/10.1016/j.physbeh.2014.04.025.

[7] P.S. Chen, Y.K. Yang, T.L. Yeh, I.H. Lee, W.J. Yao, N.T. Chiu, R.B. Lu, Correlation between body mass index and striatal dopamine transporter availability in healthy volunteers-A SPECT study, Neuroimage 40 (2008) 275–279, https://doi.org/10.1016/j.neuroimage.2007.11.007.

[8] A. Del Parigi, J.-F. Gautier, K. Chen, A.D. Salbe, E. Ravussin, P.A. Tataranni, Neuroimaging and obesity: mapping the brain responses to hunger and satiation in humans using positron emission tomography, Ann. N. Y. Acad. Sci. 967 (2002) 389–397, https://doi.org/10.1111/j.1749-6632.2002.tb04294.x.

[9] S. Kullmann, M.F. Callaghan, M. Heni, N. Weiskopf, K. Scheffler, H.U. Häring, A. Fritsche, R. Veit, H. Preissl, Specific white matter tissue microstructure changes associated with obesity, Neuroimage 125 (2016) 36–44, https://doi.org/10.1016/j.neuroimage.2015.10.006.

[10] Y. Assaf, O. Pasternak, Diffusion tensor imaging (DTI)-based white matter mapping in brain research: a review, J. Mol. Neurosci. 34 (2008) 51–61, https://doi.org/10.1007/s12031-007-0029-0.

[11] H.K. Karlsson, J.J. Tuulari, J. Hirvonen, V. Lepomäki, R. Parkkola, J. Hiltunen, J.C. Hannukainen, M. Soinio, T. Pham, P. Salminen, P. Nuutila, L. Nummenmaa, Obesity is associated with white matter atrophy: a combined diffusion tensor imaging and voxel-based morphometric study, Obesity 21 (2013) 2530–2537, https://doi.org/10.1002/oby.20386.

[12] J.D. Bolzenius, D.H. Laidlaw, R.P. Cabeen, T.E. Conturo, A.R. McMichael, E.M. Lane, J.M. Heaps, L.E. Salminen, L.M. Baker, J. Gunstad, R.H. Paul, Impact of body mass index on neuronal fiber bundle lengths among healthy older adults, Brain Imag. Behav. 7 (2013) 300–306, https://doi.org/10.1007/s11682-013-9230-7.

[13] K.M. Stanek, S.M. Grieve, A.M. Brickman, M.S. Korgaonkar, R.H. Paul, R.A. Cohen, J.J. Gunstad, Obesity is associated with reduced white matter integrity in otherwise healthy adults, Obesity 19 (2011) 500–504, https://doi.org/10.1038/oby.2010.312.

[14] B. Park, J. Seo, J. Yi, H. Park, Structural and functional brain connectivity of people with obesity and prediction of body mass index using connectivity, PLoS One 10 (2015), https://doi.org/10.1371/journal.pone.0141376 e0141376.

[15] M.A. Lips, M.A. Wijngaarden, J. Van Der Grond, M.A. Van Buchem, G.H. De Groot, H. Pijl, I.M. Veer, Resting-state functional connectivity of brain regions involved in cognitive control , motivation , and reward is enhanced in obese, Am. J. Clin. Nutr. 100 (2014) 524–531, https://doi.org/10.3945/ajcn.113.080671.1.

[16] D. Val-Laillet, E. Aarts, B. Weber, M. Ferrari, V. Quaresima, L.E. Stoeckel, M. Alonso-Alonso, M. Audette, C.H. Malbert, E. Stice, Neuroimaging and neuromodulation approaches to study eating behavior and prevent and treat eating disorders and obesity, Neuroimage Clin. 8 (2015) 1–31, https://doi.org/10.1016/j.nicl.2015.03.016.

[17] M.P. van den Heuvel, H.E. Hulshoff Pol, Exploring the brain network: a review on resting-state fMRI functional connectivity, Eur. Neuropsychopharmacol. 20 (2010) 519–534, https://doi.org/10.1016/j.euroneuro.2010.03.008.

[18] S.H. Hojjati, A. Ebrahimzadeh, A. Khazaee, A. Babajani-Feremi, Predicting conversion from MCI to AD by integrating rs-fMRI and structural MRI, Comput. Biol. Med. 102 (2018) 30–39, https://doi.org/10.1016/j.compbiomed.2018.09.004.

[19] Y. Koush, M.J. Rosa, F. Robineau, K. Heinen, S.W. Rieger, N. Weiskopf, P. Vuilleumier, D. Van De Ville, F. Scharnowski, Connectivity-based neurofeedback: dynamic causal modeling for real-time fMRI, Neuroimage 81 (2013) 422–430, https://doi.org/10.1016/j.neuroimage.2013.05.010.

[20] C.B. JS Damoiseaux, S.A.R.B. Rombouts, F. Barkhof, P. Scheltens, C.J. Stam, Stephen M. Smith, Consistent resting-state networks across healthy subjects, Proc. Natl. Acad. Sci. Unit. States Am. 103 (2006) 13848–13853, https://doi.org/10.1073/pnas.0601417103.

[21] J.R. Gawryluk, E.L. Mazerolle, R.C.N. D'Arcy, Does functional MRI detect activation in white matter? A review of emerging evidence, issues, and future directions, Front. Neurosci. 8 (2014) 1–12, https://doi.org/10.3389/fnins.2014.00239.

[22] J.R. Gawryluk, E.L. Mazerolle, K.D. Brewer, S.D. Beyea, R.C.N. D'Arcy, Investigation of fMRI activation in the internal capsule, BMC Neurosci. 12 (2011), https://doi.org/10.1186/1471-2202-12-56.

[23] E.L. Mazerolle, J.R. Gawryluk, K.N.H. Dillen, S.A. Patterson, K.W. Feindel, S.D. Beyea, M.T.R. Stevens, A.J. Newman, M.H. Schmidt, R.C.N. D'Arcy, Sensitivity to white matter fMRI activation increases with field strength, PLoS One 8 (2013), https://doi.org/10.1371/journal.pone.0058130 e58130.

[24] R.C.N. D'Arcy, A. Hamilton, M. Jarmasz, S. Sullivan, G. Stroink, Exploratory data analysis reveals visuovisual interhemispheric transfer in functional magnetic resonance imaging, Magn. Reson. Med. 55 (2006) 952–958, https://doi.org/10.1002/mrm.20839.

[25] Z. Ding, A.T. Newton, R. Xu, A.W. Anderson, V.L. Morgan, J.C. Gore, Spatio-temporal correlation tensors reveal functional structure in human brain, PLoS One 8 (2013), https://doi.org/10.1371/journal.pone.0082107.

[26] Z. Ding, R. Xu, S.K. Bailey, T.-L. Wu, V.L. Morgan, L.E. Cutting, A.W. Anderson, J.C. Gore, Visualizing functional pathways in the human brain using correlation

tensors and magnetic resonance imaging, Magn. Reson. Imaging 34 (2016) 8–17, https://doi.org/10.1016/j.mri.2015.10.003.
[27] K.B. Nooner, S.J. Colcombe, R.H. Tobe, M. Mennes, M.M. Benedict, A.L. Moreno, L.J. Panek, S. Brown, T.T. Zavitz Stephen, Q. Li, S. Sikka, D. Gutman, S. Bangaru, R.T. Schlachter, S.M.K. Anwar, C.M. Hinz, M.S. Kaplan, A.B. Rachlin, S. Adelsberg, B. Cheung, R. Khanuja, C. Yan, C.C.C. Courtney, M. King, D. Wood, C.L. Cox, A.M.C. Kelly, E. Petkova, P.T. Reiss, N. Duan, D. Thomsen, B. Biswal, B. Coffey, M.J. Hoptman, D.C. Javitt, N. Pomara, J.J. Sidtis, H.S. Koplewicz, F.X. Castellanos, B.L. Leventhal, M.P. Milham, The NKI-Rockland sample: a model for accelerating the pace of discovery science in psychiatry, Front. Neurosci. 6 (2012) 1–11, https://doi.org/10.3389/fnins.2012.00152.
[28] Obesity and Overweight, World Heal. Organ, 2016.
[29] M. Jenkinson, C.F. Beckmann, T.E.J. Behrens, M.W. Woolrich, S.M. Smith, Fsl, Neuroimage. 62 (2012) 782–790, https://doi.org/10.1016/j.neuroimage.2011.09.015.
[30] R.W. Cox, AFNI: software for analysis and visualization of functional magnetic resonance neuroimages, Comput. Biomed. Res. 29 (1996) 162–173, https://doi.org/10.1006/cbmr.1996.0014.
[31] R. Wang, T. Benner, A.G. Sorensen, V.J. Wedeen, Diffusion Toolkit : a software package for diffusion imaging data processing and tractography, Proc. Intl. Soc. Magn. Reson. Med. 15 (2007) 3720.
[32] A.J. Schwarz, J. McGonigle, Negative edges and soft thresholding in complex network analysis of resting state functional connectivity data, Neuroimage 55 (2011) 1132–1146, https://doi.org/10.1016/j.neuroimage.2010.12.047.
[33] P.J. Basser, S. Pajevic, Statistical artifacts in diffusion tensor MRI (DT-MRI) caused by background noise, Magn. Reson. Med. 44 (2000) 41–50, https://doi.org/10.1002/1522-2594(200007)44:1<41::AID-MRM8>3.0.CO;2-O.
[34] Y. Zhou, H. Zhang, L. Zhang, X. Cao, R. Yang, Q. Feng, P.T. Yap, D. Shen, Functional MRI registration with tissue-specific patch-based functional correlation tensors, Hum. Brain Mapp. (2018) 1–14, https://doi.org/10.1002/hbm.24021.
[35] S. Mori, K. Oishi, H. Jiang, L. Jiang, X. Li, K. Akhter, K. Hua, A.V. Faria, A. Mahmood, R. Woods, A.W. Toga, G.B. Pike, P.R. Neto, A. Evans, J. Zhang, H. Huang, M.I. Miller, P. van Zijl, J. Mazziotta, Stereotaxic white matter atlas based on diffusion tensor imaging in an ICBM template, Neuroimage 40 (2008) 570–582, https://doi.org/10.1016/j.neuroimage.2007.12.035.
[36] R. Tibshirani, Regression shrinkage and selection via the lasso, J. R. Stat. Soc. - Ser. D 58 (1996) 267–288.
[37] C.A. Raji, A.J. Ho, N.N. Parikshak, J.T. Becker, O.L. Lopez, L.H. Kuller, X. Hua, A.D. Leow, A.W. Toga, P.M. Thompson, Brain structure and obesity, Hum. Brain Mapp. 31 (2010) 353–364, https://doi.org/10.1002/hbm.20870.
[38] S. Gazdzinski, J. Kornak, M.W. Weiner, J. Meyerhoff, Body Mass Index and Magnetic Resonance Markers of Brain Integrity in Adults 63 (2008) 652–657, https://doi.org/10.1002/ana.21377.
[39] I. Papageorgiou, L.G. Astrakas, V. Xydis, G.A. Alexiou, P. Bargiotas, L. Tzarouchi, A.K. Zikou, D.N. Kiortsis, M.I. Argyropoulou, Abnormalities of brain neural circuits related to obesity: a Diffusion Tensor Imaging study, Magn. Reson. Imaging 37 (2017) 116–121, https://doi.org/10.1016/j.mri.2016.11.018.
[40] J. Xu, Y. Li, H. Lin, R. Sinha, M.N. Potenza, Body mass index correlates negatively with white matter integrity in the fornix and corpus callosum: a diffusion tensor imaging study, Hum. Brain Mapp. 34 (2013) 1044–1052, https://doi.org/10.1002/hbm.21491.
[41] T. Verstynen, A. Weinstein, W. Schneider, J. Jakicic, D. Rofey, K.I. Erickson, Increased body mass index is associated with a global and distributed decrease in white matter microstructural integrity, Psychosom. Med. 74 (2012) 682–690, https://doi.org/10.1097/PSY.0b013e318261909c.Increased.
[42] K. Mueller, A. Anwander, H.E. Möller, A. Horstmann, J. Lepsien, F. Busse, S. Mohammadi, M.L. Schroeter, M. Stumvoll, A. Villringer, B. Pleger, Sex-dependent influences of obesity on cerebral white matter investigated by diffusion-tensor imaging, PLoS One 6 (2011), https://doi.org/10.1371/journal.pone.0018544.
[43] L. Zhang, H. Zhang, X. Chen, Q. Wang, P.T. Yap, D. Shen, Learning-based structurally-guided construction of resting-state functional correlation tensors, Magn. Reson. Imaging 43 (2017) 110–121, https://doi.org/10.1016/j.mri.2017.07.008.
[44] X. Chen, H. Zhang, L. Zhang, C. Shen, S.W. Lee, D. Shen, Extraction of dynamic functional connectivity from brain grey matter and white matter for MCI classification, Hum. Brain Mapp. 38 (2017) 5019–5034, https://doi.org/10.1002/hbm.23711.
[45] N. Japkowicz, S. Stephen, The class imbalance problem A systematic study, Intell. Data Anal. 6 (2002) 429–449.
[46] K.J. Rothman, BMI-related errors in the measurement of obesity, Int. J. Obes. 32 (2008) S56–S59, https://doi.org/10.1038/ijo.2008.87.